Metabolism 175 (2026) 156439

Contents lists available at ScienceDirect

Metabolism

journal homepage: www.journals.elsevier.com/metabolism

Induction of Yin Yang 1 (YY1) overexpression in mature adipocytes promotes dysfunctional adipose tissue and systemic insulin resistance in mice

Line Pedersen [a,b,1], Christy M. Gliniak [a,c,1], Thomas Myhre Dale [b], Qingzhang Zhu [a,g], Chao Li [a], Jan-Bernd Funcke [a], Clair Crewe [a,d,e], Jiahui Luo [a], Lauren Palluth [a], Yi Zhu [a,f], Philipp E. Scherer [a,*]

[a] Touchstone Diabetes Center, University of Texas Southwestern Medical Center, Dallas, TX, United States of America
[b] Institute for Biomedicine, University of Bergen, Bergen, Norway
[c] Department of Nutritional Sciences, Rutgers, The State University of New Jersey, New Brunswick, United States of America
[d] Department of Cell Biology and Physiology, Washington University School of Medicine, St. Louis, MO, United States of America
[e] Department of Internal Medicine, Division of Endocrinology, Metabolism and Lipid Research, Washington University School of Medicine, St. Louis, MO, United States of America
[f] Department of Pediatrics, Baylor College of Medicine, Houston, TX, United States of America
[g] Barnstable Brown Diabetes and Obesity Center, University of Kentucky, Lexington, KY, United States of America

ARTICLE INFO

Keywords:
YY1
Adipose tissue
White adipose tissue
Adipogenesis
Obesity

ABSTRACT

The ubiquitous transcription factor Ying Yang 1 (YY1) plays a fundamental role in multiple biological processes and is believed to regulate up to 10 % of all human genes. In thermogenic brown adipose tissue, YY1 has been linked to controlling mitochondrial gene expression and regulating cellular oxidative respiration, protecting against diet-induced obesity and alterations in energy balance. The role of YY1 in non-thermogenic, white adipose tissue, on the other hand, remains largely unknown. Here, we show that adipocyte-specific induction of YY1 promotes dysfunctional adipose tissue and systemic insulin resistance in mice. Long-term YY1 induction in mature adipocytes leads to reduced weight gain, systemic insulin resistance, and increased liver steatosis in comparison to control littermates. In contrast, brown adipose tissue-specific YY1 overexpression has little effect on mice fed a high-fat diet. In an obesogenic environment, acute ectopic adiponectin promoter-driven YY1 expression promotes weight loss, cell death, and adipose tissue inflammation. Underlying the observed reduction in adipose tissue mass, we find that YY1 controls gene networks related to adipose tissue expansion, lipid anabolic pathways (hypertrophy), and hyperplasia (adipogenesis). Taken together, our results demonstrate novel roles of *Yy1* in white adipose tissue. This versatile transcription factor regulates central aspects of white adipose tissue biology that are essential for maintaining whole-body physiology.

1. Introduction

YY1 is a multifunctional transcription factor belonging to the Kruppel-like (KLI) family of transcription factors. Since its discovery in 1991, YY1 has been implicated in a plethora of cellular processes ranging from cellular proliferation, apoptosis, cell cycle progression, differentiation, replication, as well as regulating mitochondrial function and metabolic pathways [1–5]. In humans, *de novo* mutations or deletions of YY1 cause global developmental delays, cognitive impairment, feeding problems, and behavioral alterations [6]. The fundamental role of YY1 in development is further illustrated in mice carrying a homozygous deletion of the gene, resulting in embryonic lethality and heterozygote embryos that display developmental defects [7].

YY1 can act as both a transcriptional activator and as a repressor, in a context-dependent manner [8]. The diverse roles of YY1 are clearly illustrated in the field of cancer biology, where it can act both as a tumor promoter and as a tumor suppressor depending on the cellular setting and interaction partners [9]. The functional flexibility of YY1 is also

* Corresponding author.
E-mail address: philipp.scherer@utsouthwestern.edu (P.E. Scherer).
[1] Equal contribution.

https://doi.org/10.1016/j.metabol.2025.156439
Received 21 May 2025; Accepted 10 November 2025
Available online 19 November 2025

linked to the fact that 10 % of all human genes contain YY1 binding motifs in their promoter regions [10,11]. Moreover, accumulating evidence shows that YY1`s modes of transcriptional control extend beyond classical DNA binding to promoter regions. YY1 can activate or repress transcription by interacting with factors involved in chromatin modification (*e.g.*, activators such as histone acyltransferases (HATs), PRMT1, and repressors including the polycomb complex and histone deacetylases (HDACs)) [12]. Additionally, YY1 can influence gene expression by regulating 3D chromatin organization through the cooperation with architectural proteins such as CCCTC-binding factor (CTCF) and Cohesin [12]. Despite broad phenotypic and mechanistic evidence linking YY1 to fundamental processes across different tissue types and diseases, insights regarding the function of YY1 in adipose tissue remain sparse, especially in the context of white adipose tissue.

White adipose tissue is vital for thermal insulation, mechanical protection, and maintaining systemic energy homeostasis. The organ serves as a fuel reservoir by storing lipids in the form of neutral triglycerides in adipocytes through the processes of lipogenesis. On the other hand, when food is limited, energy requirements are elevated, or the storage capacity of adipocytes is surpassed, adipose tissue controls energy mobilization through the breakdown of triglycerides to free fatty acids and glycerol by lipolysis. Under conditions where the amount of adipose tissue is limited (*e.g.* in lipodystrophic states) or dysfunctional (*e.g.*, obesity), lipids start infiltrating non-adipose tissues, such as the liver and muscles. Lipid accumulation in non-adipose tissues is a major contributor to insulin resistance, which again could contribute to the progression to type 2 diabetes and related pathologies [13,14]. Adipose tissue is, furthermore, a highly active endocrine organ, secreting factors that mediate inter-organ communication and play functional roles in the metabolic status of the system as well as inflammatory processes.

To date, two independent reports have studied the effects of adipocyte-specific depletion of YY1 [15,16]. Both studies find that lack of YY1 in adiponectin-expressing cells protects against diet-induced obesity and leads to metabolic improvements. Furthermore, the knock-out studies show that YY1 regulates mitochondrial function and thermogenic capacity of beige/brown adipocytes. Discrepancies exist between the studies regarding the role of YY1 in regulating energy balance, and consequently, they propose different mechanisms

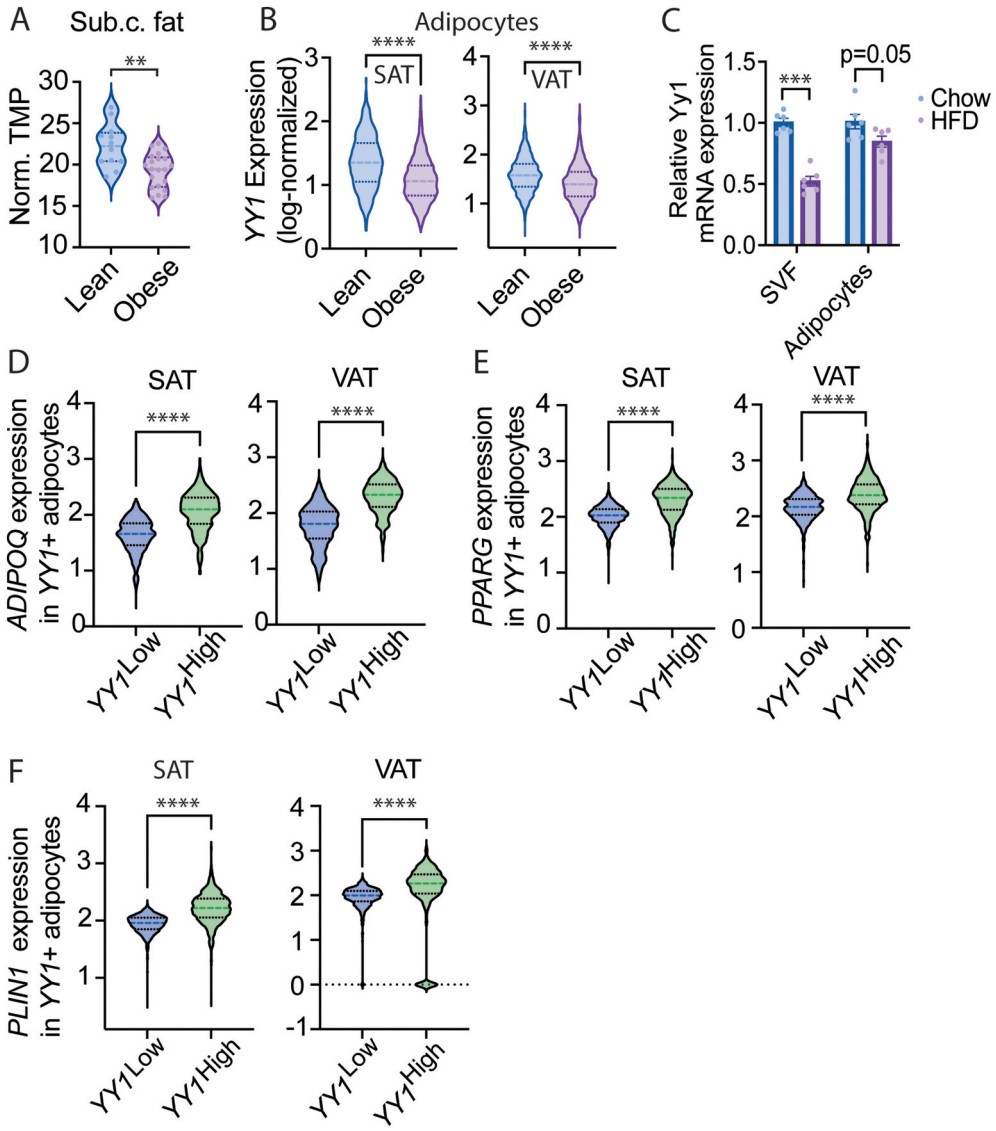

Fig. 1. *YY1* levels are reduced in human and mouse white adipose tissue during obesity. **A)** *YY1* expression in subcutaneous tissue from lean ($n = 12$) and obese ($n = 21$) humans. Data was extracted from [32] and is presented as normalized Transcripts Per kilobase Million (TPM). B) Log-normalized *YY1* expression in adipocytes isolated from subcutaneous adipose tissue (SAT) and visceral adipose tissue (VAT). Data was extracted from [17]. **C)** Relative *Yy1* mRNA expression in SVF and floated adipocytes harvested from male mice fed a regular chow ($n = 5$) or HFD ($n = 6$) for 10 weeks. Data is presented as mean ± SEM. **D—F)** Log-normalized expression of *ADIPOQ*, *PPARG* and *PLIN1* in *YY1*-positive human adipocytes with low *versus* high *YY1* expression extracted from SAT and VAT [17].

underlying the observed phenotypes.

The aim of this study was to determine the effect of YY1 induction in adipocytes. Since YY1 regulates embryogenesis and cellular differentiation, congenital mouse models are not ideal for the study of YY1 *in vivo*. Therefore, we developed transgenic mice that overexpress YY1 in a doxycycline-inducible, tissue-specific manner, *i.e.* in mature adipocytes, driven by the adiponectin promoter. We find that long-term ectopic YY1 expression in adult mice restricts adipose tissue expansion, causing lipotoxicity and metabolic defects.

2. Results

2.1. YY1 levels are reduced in human and mouse white adipose tissue during obesity

In human white adipose tissue, Y*Y1* is expressed in pre-adipocytes as well as in mature adipocytes [17] (**Supplementary Fig. 1 A**). *YY1* expression levels are regulated in response to obesity. In subcutaneous white adipose tissue, *YY1* levels are lower in obese *versus* lean individuals (Fig. 1A). Similarly, YY1 expression is reduced upon obesity in adipocytes isolated from both visceral and subcutaneous human depots [17] (Fig. 1B). We also observed a similar trend in mice, as *Yy1* levels were reduced in wild-type mice fed a high-fat diet (HFD) compared to stromal vascular cells and adipocytes isolated from chow-fed littermates (Fig. 1C). Further exploration of *YY1* expression patterns in a human transcriptomic single-cell transcriptomic dataset [17], revealed that adipocyte-specific *YY1* expression levels correlate with expression of canonical markers of mature adipocytes (*ADIPOQ, PPARG* and *PLIN1*), part of the core adipocyte transcriptional program **(Supplementary Fig. 1B,** Fig. 1D-F**).** Together, these findings highlight YY1 as a transcriptional regulator that is sensitive to metabolic state and suggest that its expression may be linked to the maintenance of adipocyte identity or function.

2.2. Long-term adiponectin-driven Yy1 induction leads to reduced weight gain, systemic insulin resistance and increased liver steatosis

To determine the effects of elevated *Yy1* levels on adipose tissue function, we utilized the tetracycline (TET)-on system to generate mice with inducible adipose tissue-specific overexpression of *Yy1* (Fig. 2A). Mice fed doxycycline-containing diets increased *Yy1* overexpression in white and brown adipose tissue depots, with no alteration of *Yy1* expression in the liver (**Supplementary Fig. 2A and B**). Interestingly, 12 weeks of *Yy1* activation led to a significant reduction in body weight for adult male mice fed a normal chow diet (Fig. 2B and C). Body composition analysis (EcoMRI) and weighing of tissues at the endpoint (12 weeks) showed a significant reduction in white adipose tissue mass in transgenic mice (Fig. 2D and E**; Supplementary Fig. 2C**). Lean mass normalized by body weight increased upon adipocyte-specific Yy1 overexpression (Fig. 2**; Supplementary Fig. 2D**).

Since *Yy1* overexpression reduces fat mass, we challenged transgenic mice with doxycycline-containing HFD. Long-term induction (Fig. 2B) led to a 3-fold *Yy1* overexpression in white adipose tissue depots and over 10-fold overexpression in brown adipose tissue (**Supplementary Fig. 2B).** Consistent with our observation in chow-fed mice**,** *Yy1* induction significantly reduced body weight gain in comparison to control mice after 6–8 weeks of HFD-feeding (Fig. 2G). EcoMRI and assessment of tissue weights at the endpoint (20 weeks) confirmed a reduction in adipose tissue mass (**Fig. 2H** and **I**). The impairment in fat mass accumulation could not be explained by altered energy balance, as the adiponectin promoter-driven *Yy1* expression did not affect energy balance as assessed by measuring food intake, O_2 consumption, CO_2 production, or respiratory exchange ratio (RER) (Fig. 2J-L**; Supplementary Fig. 2E).** Despite being protected against HFD-induced weight gain, mice with *Yy1* overexpression were glucose intolerant and insulin resistant compared to control animals, as determined by glucose and insulin tolerance tests (Fig. 2M and N**).** However, mice with *Yy1* overexpression fed a chow diet displayed no changes in glucose intolerance (**Supplementary Fig. 2F)**. Glucose-stimulated insulin secretion increased upon *Yy1* expression levels on chow, but not on HFD (Fig. 2O**; Supplementary Fig. 2G**). At the histological level, adipocytes appeared smaller and of more irregular shape in eWAT and SWAT from transgenic mice in comparison to control mice fed either HFD or chow (Fig. 2P**; Supplementary Fig. 2H**). Overall, the data suggest that adipocyte-specific *Yy1* overexpression promotes the generation of unhealthy adipose tissue.

We further examined the systemic effects of *Yy1* overexpression in obese mice. Previous studies suggest that Yy1 regulates circulating levels of adipose-derived factors, such as Fibroblast Growth Factor 21 (FGF21) [15]. FGF21 levels remained unaltered compared to control mice. A major downstream target of FGF21, adiponectin, remained unchanged. However, leptin levels were significantly reduced upon *Yy1* induction (Fig. 2Q-2S). Evaluation of liver histology and liver mass at the endpoint revealed an increased lipid deposition in non-adipose tissues for HFD-fed transgenic mice, but not for chow-fed mice (Fig. 2F, T and U**; Supplementary Fig. 2I**). Gene expression for markers of liver fibrosis increased in the liver in the HFD-fed transgenic mice group, but for the chow–fed group (**Supplementary Fig. 2J and 2K)**. Despite the liver steatosis caused by adipocyte-specific Yy1 overexpression on a HFD, hepatic expression for key liver enzymes were not changed (**Supplementary Fig. 2L and 2M)**. In addition, immune markers did not increase in transgenic mice from either the chow or HFD diet groups (**Supplementary Fig. 2L and 2M)**. Taken together, adipocyte-specific expression of *Yy1* leads to reduced white adipose tissue mass, reduced local lipid storage, and the induction of systemic insulin-resistance.

2.3. No significant systemic impact of BAT-specific Yy1 overexpression in obese mice

As previously reported, brown adipose tissue YY1 deficiency prevented diet-induced obesity through increasing energy expenditure by regulating mitochondrial respiration and secretion of factors linked to energy expenditure [15]. We therefore sought to determine the relative contribution of elevated YY1 expression in BAT on the phenotype observed in mice with *Yy1* expression from the adiponectin promoter, which is also active in brown adipocytes. Adipocyte-specific inducible *Yy1* expression led to a 40-fold induction in mRNA levels in brown adipose tissue (Fig. 3A). Although brown adipose tissue weight did not differ between the transgenic and control mice on a HFD (Fig. 2I), histological assessment revealed a significant whitening of brown adipose tissue in transgenic mice compared to controls (Fig. 3B).

To further understand the role of YY1 specifically in BAT, we crossed TRE-*Yy1* mice with mice expressing the reverse tetracycline-controlled transactivator (rtTA) protein under the control of the brown adipocyte specific promoter Ucp1 (Fig. 3C). We followed an identical experimental setup for the mice with long-term adiponectin-driven *Yy1* expression on HFD (Fig. 3D). A five-fold increase in *Yy1* mRNA levels was detected in brown adipose tissue after 20 weeks of HFD feeding (Fig. 3E). At this point, transgenic mice could be identified by a major enlargement of their interscapular brown adipose tissue, and histological assessment showed an increased whitening (Fig. 3F). However, BAT-specific overexpression of *Yy1* did not cause any overall changes in body weight (Fig. 3G). Assessment of body composition revealed an increase in fat mass upon *Yy1* expression (Fig. 3H), which could be attributed to the observed increase in brown adipose tissue mass (Fig. 3I). In metabolic tests, Ucp1-*Yy1* mice performed comparable to control mice (Fig. 3J and K).

We also tested whether adiponectin-driven *Yy1* overexpression leads to metabolic dysfunction in a thermoneutral environment, where brown adipose tissue activity is minimized. Upon long-term feeding with doxycycline containing HFD, transgenic mice displayed a reduced weight gain and adipose mass to a similar extent as the mice at room

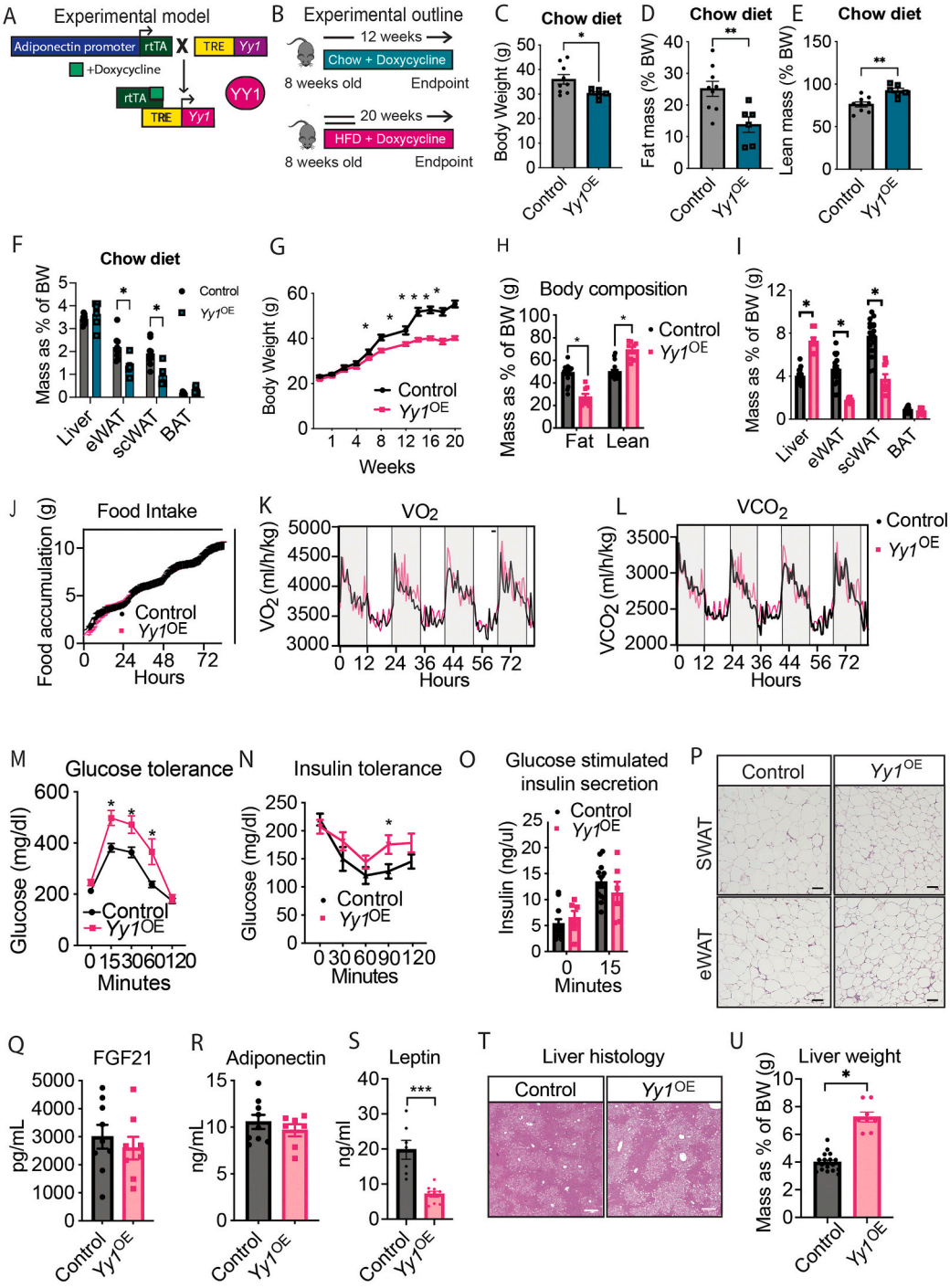

Fig. 2. Long-term adiponectin-driven *Yy1* induction leads to reduced weight gain, systemic insulin resistance and increased liver steatosis. **A)** Schematics of the TET-on inducible expression system employed. For experiments, all mice were positive for adiponectin- tetracycline-controlled transactivator (rtTA) and whereas *Yy1*^{OE} mice were heterozygous for Tet Response Element (TRE)-*Yy1*. **B)** Outline of experiments designed to study the long-term effect of *Yy1* expression in adult male mice fed a standard chow-diet containing 600 mg/kg doxycycline (C-E) or fed a high-fat diet (60 %kcal from fat) containing 600 mg/kg doxycycline (G-T). **C—F)** Control ($n = 9$) and *Yy1*^{OE} ($n = 6$) mice were fed a chow-doxycycline diet for 20 weeks. Body weight (C), Body composition determined by Eco-MRI presented as % of total body weight for fat mass (D) and lean mass (E), and tissue weights of liver and adipose depots. **G-I)** Control mice ($n = 17$) and *Yy1*^{OE} mice ($n = 8$) fed high-fat diet (60 %kcal from fat) containing 600 mg/kg doxycycline. Bi-weekly body weights measurements (G), Body composition determined by Eco-MRI and fat and lean mass presented as % of total body weight at experimental endpoint (H), Tissue mass of indicated organs at experimental endpoint (I). **J-L)** Food intake (J), VO_2 consumption (K), and VCO_2 consumption (L) measurements performed in control ($n = 6$) and *Yy1*^{OE} mice ($n = 6$) 4 weeks on doxycycline-containing HFD. Data is presented as mean. **M)** Oral glucose tolerance test performed on control (n = 17) and *Yy1*^{OE} mice ($n = 8$) 16 weeks post-*Yy1* induction. **N)** Intraperitoneal insulin tolerance of *Yy1*^{OE} mice ($n = 6$) and control littermates ($n = 12$) performed on mice fed HFD-Doxycycline for 14 weeks. **O)** Glucose stimulated insulin secretion measured 15 min after glucose administration in control ($n = 17$) and *Yy1*^{OE} mice ($n = 8$) fed HFD-Doxycycline for 16 weeks. **P-R)** Circulating FGF21 (P), adiponectin (Q), and leptin (R) levels measured in blood collected from control and *Yy1*^{OE} mice fasted overnight after 20 weeks of HFD-Doxycycline feeding. $n = 7$–9 mice per group. **S)** Liver histology was assessed by H&E staining at experimental endpoint in control and *Yy1*^{OE} mice (20 weeks post YY1 induction). Scalebar = 50 μm. **T)** Liver weight at experiment endpoint, presented in relation to bodyweight. Control mice, $n = 17$. *Yy1*^{OE} mice, $n = 8$. Unless otherwise stated, data in Fig. 1 is presented as mean ± SEM. Differences were considered significant when $p > 0.05$.

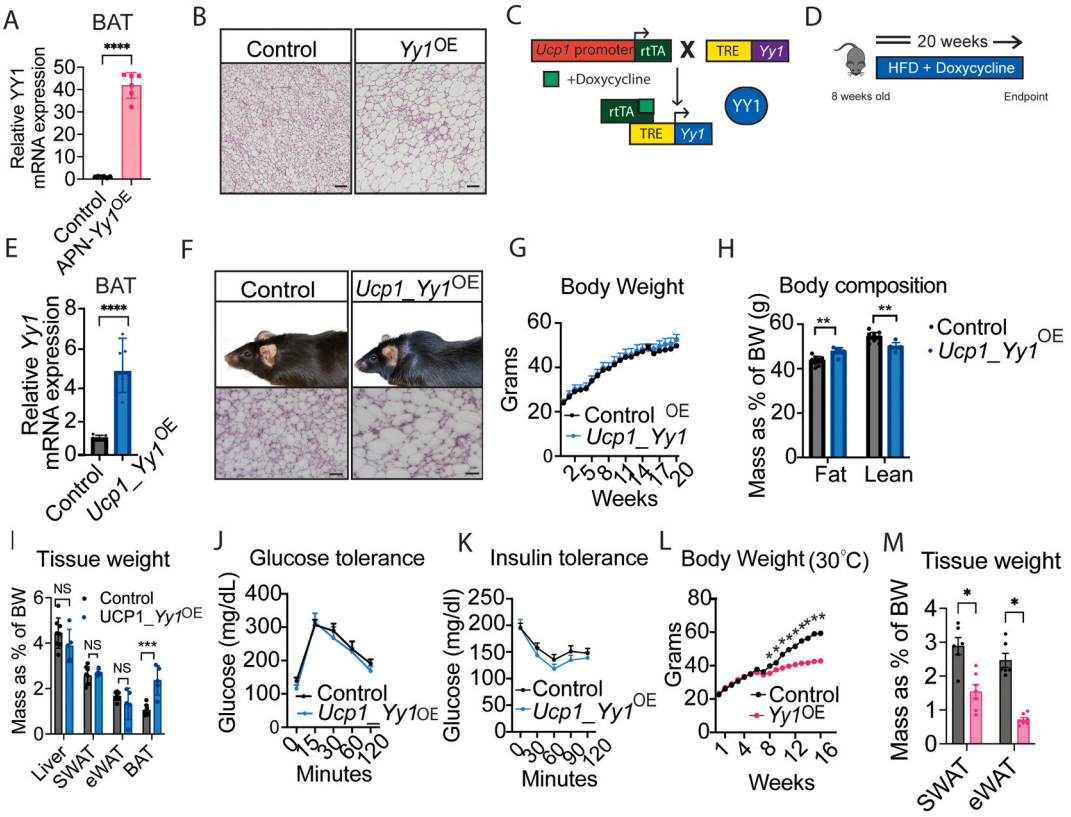

Fig. 3. BAT specific *Yy1* overexpression during obesity does not alter glucose metabolism. **A)** *Yy1* mRNA expression in BAT collected from mice with adiponectin-driven *Yy1* overexpression ($n = 6$) and controls ($n = 6$) at experimental endpoint (20 weeks). **B)** H&E staining of BAT collected after 20 weeks HFD-doxycycline feeding of control and adiponectin – $Yy1^{OE}$ mice. Scalebar =50 μm. **C)** Schematics of the TET-on inducible expression system employed to overexpress *Yy1* specifically in brown adipocytes using the *Ucp1* promoter. **D)** Experimental outline for characterization of *Ucp1-*$Yy1^{OE}$ mice. **E)** Relative *Yy1* mRNA expression in BAT at experimental endpoint (20 weeks) of controls ($n = 6$) and mice with *Ucp1*-driven *Yy1* expression ($n = 5$). **F)** Upper panel: Transgenic mice could be identified by a major enlargement of the interscapular brown adipose tissue depot. Lower panel: H&E staining of BAT collected after 20 weeks HFD-doxycycline feeding of control and *Ucp1*–$Yy1^{OE}$ mice. **G)** Bi-weekly body weights measurements of control ($n = 8$) and $Yy1^{OE}$ mice ($n = 6$) post HFD-Doxycycline feeding. **H)** Body composition determined by Eco-MRI presented as % of total body weight at experimental endpoint (20 weeks feeding). For control/*Ucp1-*$Yy1^{OE}$ $n = 8/5$ mice. **I)** Tissue mass of indicated organs at experimental endpoint. Controls $n = 8$ mice, *Ucp1-* $Yy1^{OE}$ $n = 5$ mice. **J)** Oral glucose tolerance test performed on control ($n = 8$) and $Yy1^{OE}$ mice ($n = 5$) 15 weeks post-*Yy1* induction. **K)** Intraperitonal insulin tolerance of $Yy1^{OE}$ mice ($n = 6$) and control littermates ($n = 8$) performed on mice fed HFD-Doxycycline for 14 weeks. **L)** Weekly body weights measurements of control ($n = 6$) and Adiponectin-rtTA x TRE-*Yy1* mice ($n = 7$) on HFD-doxycycline, housed in a thermoneutral environment (30 °C). **M)** Tissue weights at experimental endpoint (20 weeks of HFD-Doxycycline feeding). Controls $n = 6$ mice, Adiponectin-rtTA x TRE-*Yy1* $n = 7$ mice. All data is presented as mean ± SEM unless otherwise stated, and differences considered significant when $p > 0.05$. (For interpretation of the references to colour in this figure legend, the reader is referred to the web version of this article.)

temperature (Fig. 2G-H; 3 L-M). We conclude that in our mouse model of adipocyte-specific *Yy1* overexpression, the metabolic phenotype is not driven by *Yy1* expression in BAT.

2.4. *Acute Yy1 expression in an obesogenic environment promotes cell death and inflammation*

To gain insights into YY1-regulated cellular pathways in adipose tissue, we studied the short-term effect of *Yy1* expression. Mice were first pre-fed a regular HFD for 8 weeks, prior to switching to doxycycline-containing HFD to induce *Yy1* expression (Fig. 4A). With this experimental design, *Yy1* expression caused initially a significant drop in body weight and fat mass compared to control mice, and subsequently the weight loss plateaued (Fig. 4B and C). A clear development of liver steatosis was observed 10 days after ectopic *Yy1* expression (Fig. 4D), suggesting an acute effect of *Yy1* induction in a pre-established obese environment. We performed RNA-seq analysis of epididymal adipose tissue collected 4 days post *Yy1*-induction **(Supplementary Fig. 3 A and B).** At this early timepoint, no significant changes in body weight were observed (Fig. 4E). Signs of altered adipocyte cellular physiology were present, as indicated by elevated circulating fasting glucose levels and decreased leptin levels (Fig. 4F and G). Differential gene expression analysis revealed 516 up-regulated and 557 down-regulated genes (FDR < 0.05) (Fig. 4H). We next performed an overrepresentation analysis of significantly dysregulated genes to identify affected pathways. Interestingly, the pathways enriched in $Yy1^{OE}$ tissues were dominated by pathways connected to immune cell activity (Fig. 4I). Gene set enrichment analysis (GSEA) furthermore showed an enrichment of genes associated with an inflammatory response, including interleukin 6 (IL-6) production (**Supplementary Fig. 4 A**). Besides acting as a traditional DNA-binding transcription factor, YY1 is known to regulate transcription through interactions with chromatin remodeling complexes that regulate transcription by regulating chromatin accessibility [12]. We therefore decided to complement our mRNA expression analysis with chromatin accessibility profiling using *Assay for Transposase-Accessible Chromatin using sequencing* (ATAC-seq). ATAC-seq was performed on adipocytes differentiated *in vitro* using stromal vascular cells collected from transgenic and control mice (**Supplementary Fig. 3C and D)**. Doxycycline was added to the culture media 6 days after adding the differentiation mixture, and cells collected for ATAC-seq on day 9 of differentiation. Oil-red-O staining showed comparable lipid accumulation between the conditions at this timepoint (Fig. 4J). Differential accessibility analysis revealed 569 peaks with increased accessibility (gain peaks), and 226

(loss peaks) peaks with decreased accessibility upon *Yy1* induction, compared to control cells (Fig. 4K). Peak annotation revealed that a small fraction of the gain peaks was located in promoter regions (3.9 %), while the majority mapped to distal intergenic regions (47.3 %). Amongst the loss peaks, 19.5 % were found in promoter regions, 31.8 % in distal intergenic regions and 40.2 % in introns (**Supplementary Fig. 4B**). Interestingly, when performing HOMER motif analysis of accessible peaks, YY1 binding sites were not amongst the enriched motifs. Instead, there was an enrichment of other well-described transcription factors important for adipocyte function, including CEBPE, CEBPA, and KL6 (**Supplementary Fig. 4C**). Integration of chromatin accessibility and gene expression data revealed 70 regions associated with genes whose expression was altered by Yy1 induction (**Supplementary Fig. 4D and E**). Consistent with upregulated mRNA transcripts in the *Yy1* overexpressing conditions, gene over-representation analysis of regions with increased chromatin accessibility revealed an enrichment of pathways associated with an inflammatory response (Fig. 4L).

To further investigate whether induction of *Yy1* triggers an immune response, we assessed mRNA expression of selected immune cell markers and cytokines in eWAT, which confirmed increased *Il6* expression (Fig. 4M). In the chow diet study (Fig. 2B), there were no alterations of immune cell markers except for a reduction of *Cd8* in

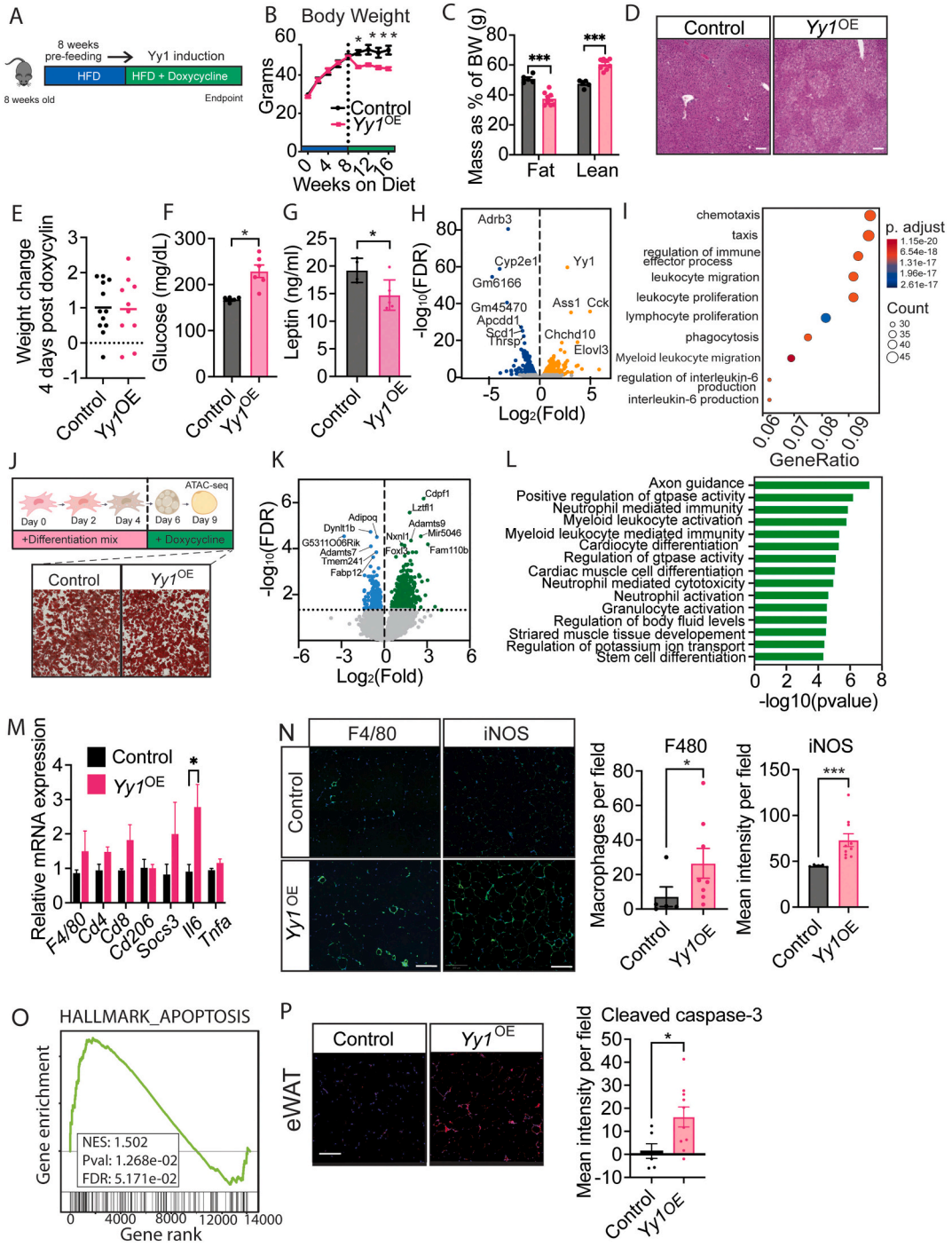

(caption on next page)

Fig. 4. Acute *Yy1* expression in an obese environment promotes cell death and inflammation. **A)** Outline of experiments designed to study the short-term effect of *Yy1* expression in obese adult male mice. Mice were pre fed a regular HFD-diet for 8 weeks, before *Yy1* expression was activated by switching to HFD containing 600 mg/kg Doxycycline (Fig. 4C-E, M). **B)** Body weight gain of transgenic mice ($n = 9$) and control littermates ($n = 5$). **C)** Body composition analysis of control ($n = 5$) and $Yy1^{OE}$ mice ($n = 8$) mice at experimental endpoint (8 weeks post-*Yy1* induction) presented as percentage of body weight. **D)** Liver histology was assessed by H&E 10 days after induction of *Yy1* expression. Scalebar = 100 μm. **E)** No difference in weight change (relative to pre-*Yy1* induction) was observed between $Yy1^{OE}$ ($n = 10$) and control mice ($n = 12$) 4 days post diet-switch. **F)** Circulating glucose levels measured 4 days post diet-switch of transgenic ($n = 6$) and control ($n = 5$) mice. **G)** Circulating leptin levels measured 5 days post diet-switch of transgenic ($n = 6$) and control ($n = 5$) mice. **H)** Volcano- plot showing deregulated genes when comparing transcriptomic profiles of adipose tissue (eWAT) collected from control ($n = 2$) and $Yy1^{OE}$ mice ($n = 2$) 4 days post-diet switch. The significant (Padjusted <0.05) upregulated genes (green circles) are represented as log2 ($Yy1^{OE}$/control) gene expression >1 and downregulated (blue circles) as log2 ($Yy1^{OE}$/control) gene expression <1-fold changes. **I)** Overrepresentation analysis of significantly upregulated genes in $Yy1^{OE}$ compared to control mice showing top 10 enriched pathways. **J)** Outline of experiments designed to study potential YY1-induced effects on chromatin accessibility by ATAC-seq in mature adipocytes. Stromal vascular cells were isolated from young transgenic and control mice and differentiated *in vitro*. *Yy1* expression was activated by adding Doxycycline to the culture media 6 days after start of differentiation. Cells were collected 3 days later, at day 9 of differentiation. No effects on lipid accumulation were observed between the conditions at this timepoint, as shown by oil-red-o stain in the lower panel of the Fig. **K)** Differential binding analysis of chromatin accessibility. Genes corresponding to gain peaks (regions with increased accessibility) are show in green, whereas loss peaks (regions with reduced accessibility) are shown in blue. Regions with a Log2 Fold >0 and FDR < 0.05 were considered differentially accessible between the two conditions. **L)** GO pathway analysis of genes with increased chromatin accessibility upon *Yy1* overexpression. **M)** Relative mRNA expression of selected immune-related genes in eWAT from control ($n = 5$) *versus* $Yy1^{OE}$ mice ($n = 5$) fed HFD-doxycycline for 20 weeks. **N)** Immunofluorescent staining and quantification of the macrophage markers F4/80 and iNOS in eWAT from control ($n = 5$) and transgenic mice ($n = 8$) collected 12 days post *Yy1*-induction. Scalebar =200 μm. **O)** Functional analysis of deregulated genes comparing the transcriptomics of eWAT from $Yy1^{OE}$ ($n = 2$) and control (n = 2) mice revealed an enrichment of genes in apoptosis related pathways. NES, normalized enrichment score; FDR, false discovery rate. **P)** Immunofluorescent staining and quantification of the apoptosis marker cleaved-caspase 3 in eWAT from control ($n = 5$) and transgenic mice ($n = 8$) collected 12 days post *Yy1*-induction. Fluorescent signal is normalized to a negative control stain. Scalebar =200 μm. (For interpretation of the references to colour in this figure legend, the reader is referred to the web version of this article.)

transgenic mice compared to control mice (**Supplementary Fig. 5 A**). As increased secretion of IL-6 from adipocytes is linked to increased macrophage infiltration in adipose tissue [18], we examined macrophage abundance in eWAT collected 10 days after *Yy1* induction. At this timepoint, the average number of macrophages per histological field was higher in transgenic mice compared to controls (26.5 *vs.* 7.1). Moreover, the mean intensity of iNOS signal was significantly higher, suggesting an increased infiltration of M1-like macrophages [19] (Fig. 4L). Given that acute *Yy1* induction induces weight-loss and that adipocyte apoptosis is a key initial event that contributes to macrophage infiltration in adipose tissue, we hypothesized that ectopic *Yy1* expression could lead to an enhanced level of adipocyte apoptosis. At the transcriptional level, we observed an enrichment of genes related to apoptotic pathways (Fig. 4O). Moreover, immunofluorescent staining for the classical apoptosis marker, cleaved caspase-3, showed an increased signal in eWAT collected from mice with high *Yy1* expression compared to control mice (Fig. 4P). Collectively, our data suggest that acute adipocyte *Yy1* expression in an obese environment may promote cell death and inflammation in adipose tissue.

2.5. A Yy1-induced decline in fat anabolic pathways reduces adipocyte size

Having established the cellular changes linked to enriched mRNA sequences and open chromatin regions, we sought to investigate the less abundant transcripts and chromatin regions with reduced accessibility. Interestingly, overrepresentation analysis performed on dysregulated transcripts *in vivo* and differentially accessible chromatin regions *in vitro* mutually suggested that pathways related to fatty acid biosynthesis are significantly downregulated upon *Yy1* expression (**Fig. 5A** and **B**). Further assessment of the group of genes comprising fatty acid metabolism-related activities showed reduced expression of several key enzymes integral for different fat anabolic pathways (**Supplementary Fig. 5B**). The reduced expression of a selection of these factors was validated by qPCR analysis of eWAT for mice of a HFD (Fig. 5C). Evaluation of these selected factors from mice in the chow-fed groups revealed only *Hsl* and *Fasn* were reduced in eWAT and *Hsl* in SWAT chow diet (**Supplementary Fig. 2O and P**). As adipocyte volume is mainly controlled by the balance between fatty acid release and storage, we speculated that adipocyte volume would be compressed in $Yy1^{OE}$ mice due to reduced storage. This was confirmed by the analysis of the histological sections in Fig. 2 from both epididymal and subcutaneous depots. Consistent with our hypothesis, long-term *Yy1* expression led to significantly smaller adipocytes as determined by adipocyte area and a larger number of adipocytes per field (Fig. 5D and E). To functionally validate that the reduced adipocyte size was predominantly the result of reduced lipogenesis in the transgenic mice, we also measured lipolytic activity. *In vitro*, glycerol release after stimulation with Forskolin or CL 316,243 was not altered in adipocytes differentiated from SVF cells obtained from TRE-*Yy1* mice in comparison to cells from control mice (Fig. 5F). Moreover, neither the level of circulating glycerol nor non-esterified fatty acids (NEFAs) was altered after CL 316,243-stimulated lipolysis *in vivo* after short-term *Yy1* induction (10 days) compared to controls (Fig. 5G). Collectively, our data suggest that YY1 reduces the capacity of mature adipocytes to store lipids, leading to lipid spillover to non-adipose tissues, such as the liver and ultimately triggering systemic metabolic dysfunction.

2.6. Yy1 regulates hyperplasia in vitro and in vivo

Having established a role of YY1 expression in connection to adipocyte viability and fatty acid metabolism in mature adipocytes, our data directed us to explore yet another mechanism that potentially underlies the reduced fat mass observed upon ectopic *Yy1* expression, namely adipocyte hyperplasia. In our long-term studies, *Yy1*-induced fat mass reduction was observed at a timepoint where hyperplasia is believed to contribute to fat expansion (*e.g.* 6–8 weeks of HFD feeding) [20] (Fig. 2G). Furthermore, our omics data showed that transcripts related to adipogenesis were significantly downregulated (Fig. 5A) and that their chromatin regions were less accessible (Fig. 5B). GSEA analysis of both mRNA data and chromatin accessibility data from TRE-*Yy1* mice and adipocytes with ectopic *Yy1* expression revealed a negative enrichment of adipogenesis-related genes compared to control mice (Fig. 6A). Moreover, when performing footprinting analysis of differentially accessible chromatin regions, we identified a set of transcription factors known to be important for early adipogenesis to be more active in $Yy1^{OE}$ cells (Fig. 6B). By assessing *Yy1* expression at mRNA and protein levels in wild-type cells and mice, we found that *Yy1* is induced during fibroblast differentiation *in vitro* and is higher in floated adipocytes compared to cells from the stromal vascular fraction (Fig. 6C, D and E). We directly tested the effect of ectopic Yy1 expression on adipocyte differentiation using our *in vitro* inducible *Yy1* expression model system. In contrast to the experiments designed to examine the role of YY1 in mature adipocytes (Fig. 4 and Fig. 5), we induced *Yy1*

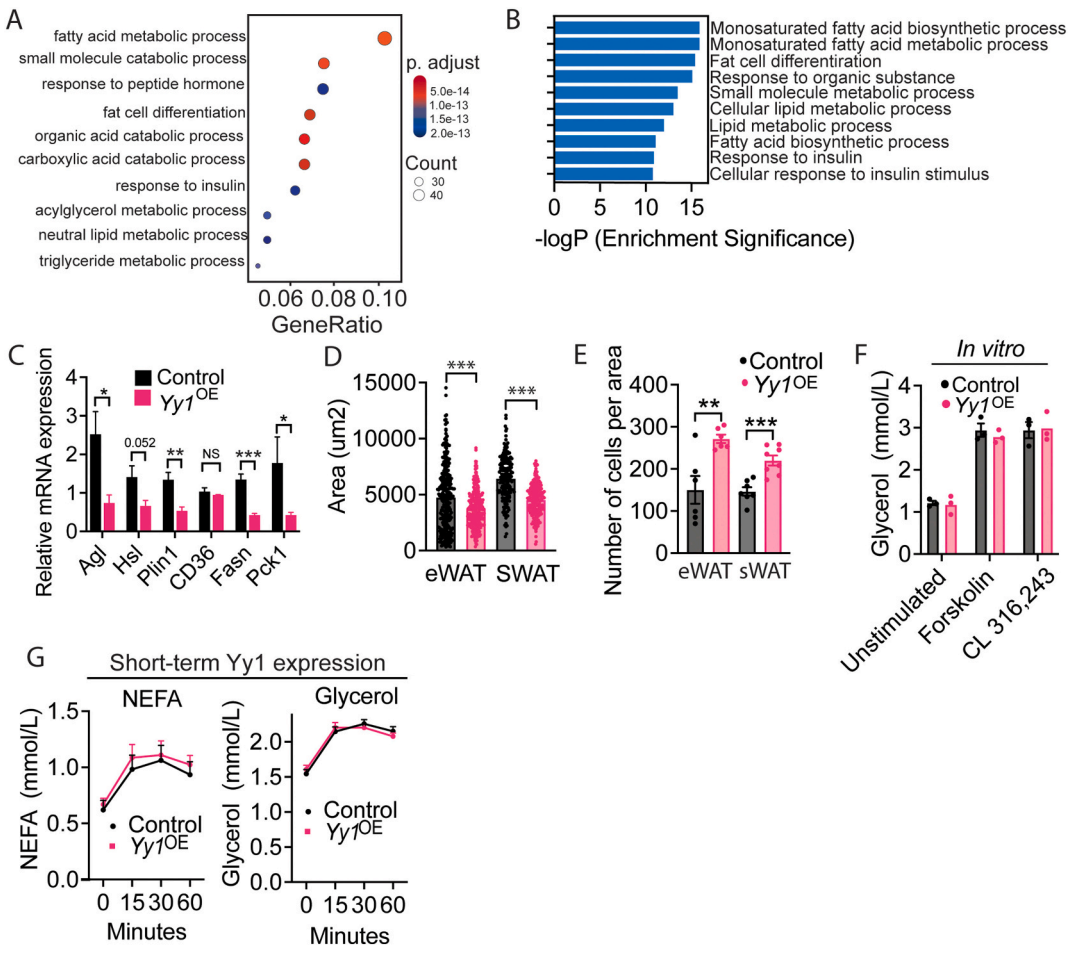

Fig. 5. Yy1-induced decline in fat anabolic pathways reduce adipocyte size. **A)** Enriched pathways identified amongst downregulated transcripts in *Yy1*^{OE} *vs* Control eWAT ($n = 2$ per group) after short-term YY1 induction in obese mice. **B)** Pathway analysis of regions with reduced chromatin accessibility in *Yy1*^{OE} adipocytes *vs.* control cells ($n = 3$ per group), as determined by ATAC-seq. **C)** Relative mRNA expression of selected fatty-acid metabolism-related genes in eWAT from control *versus* *Yy1*^{OE} mice ($n = 5$). **D)** Adipocyte size measured in eWAT and SWAT after long-term *Yy1* expression (20 weeks) in mice fed HFD, $n = 6$ mice per group. Scalebar 100 μm. **E)** Glycerol levels measured in culture media 4 h after lipolysis stimulus. Control/*Yy1*^{OE} $n = 3$. **F)** Beta-3 adrenergic receptor agonist (CL 316,243) stimulated NEFA and glycerol release measured in obese mice after short-term (5 days) *Yy1* expression ($n = 4$–6).

expression at an earlier stage by adding doxycycline to the culture medium at the time of differentiation initiation (Day 0) (Fig. 6F). With this experimental setup, it was clear that *Yy1* expression led to a reduction in lipid accumulation as assessed by Oil-red-O staining on Day 10 (Fig. 6G and H).

Lastly, to determine the relative contribution of YY1-induced hyperplasia reduction *in vivo*, we assessed the effect of high *Yy1* levels on adipocyte differentiation during developmental-related hyperplasia. Ectopic *Yy1* expression was induced by doxycycline administration on embryonic day 13 (E13) by supplying it through the food of the pregnant dam (Fig. 6I). Histological evaluation at postnatal day 7 (P7) showed clearly *Yy1*-induced defects in all tissues examined (SWAT, BAT and liver) **(**Fig. 6J**).** In contrast to the uniform appearance in control mice, adipocytes in white adipose tissues from transgenic mice appeared to be of irregular size. Furthermore, *Yy1* expression caused a significant whitening of brown adipose tissue and hepatic lipid accumulation (Fig. 6J). Taken together, the data suggest that YY1 levels need to be tightly controlled during adipogenesis and that especially the early phase is sensitive to alterations mediated by YY1-regulated signaling. The data also stresses the importance of inducing YY1 in adult mice for metabolic studies, avoiding any potential confounding developmental effects.

2.7. Transcriptional responses induced by ectopic YY1 expression are only to a minor extent mediated through direct binding to promoter regions

Our data suggest that manipulation of *Yy1* levels *in vivo* and *in vitro* affects several processes vital for adipocyte biology. Lastly, we questioned whether any of these effects are related to differential DNA-binding patterns to promoter regions of essential key players, or whether it is more likely that the observed phenotype upon ectopic expression is the result of other indirect modes of YY1-regulated transcription (*e.g.* at the level of chromatin or interaction partners). To determine YY1-DNA binding patterns, we employed our *in vitro* model system to study *Yy1* induction in mature adipocytes (Fig. 4J) and performed *Cleavage Under Targets & Release Using Nuclease* (CUT&RUN) assays (**Supplementary Fig. 3E-3F**). When studying the genome-wide occupancy patterns, we identified 7595 shared peaks between samples with endogenous and ectopic *Yy1* expression. *Yy1* overexpression caused a significant further enrichment of 1589 regions (FDR < 0.05) (Fig. 7A). For both conditions, *de novo* motif discovery analysis revealed an enrichment of the YY1 motif (Fig. 7B). Peak annotation showed that upon *Yy1* overexpression, gain peaks mapped more frequently to distal intergenic regions (17.9 % *versus* 10.9 %) and introns (17.3 % *versus* 7.75 %) and less frequently to promoter regions (61.5 % *versus* 78.7 %) in comparison to the control setting (Fig. 7C). To understand whether the differential DNA-binding patterns upon *Yy1*^{OE} could reflect the

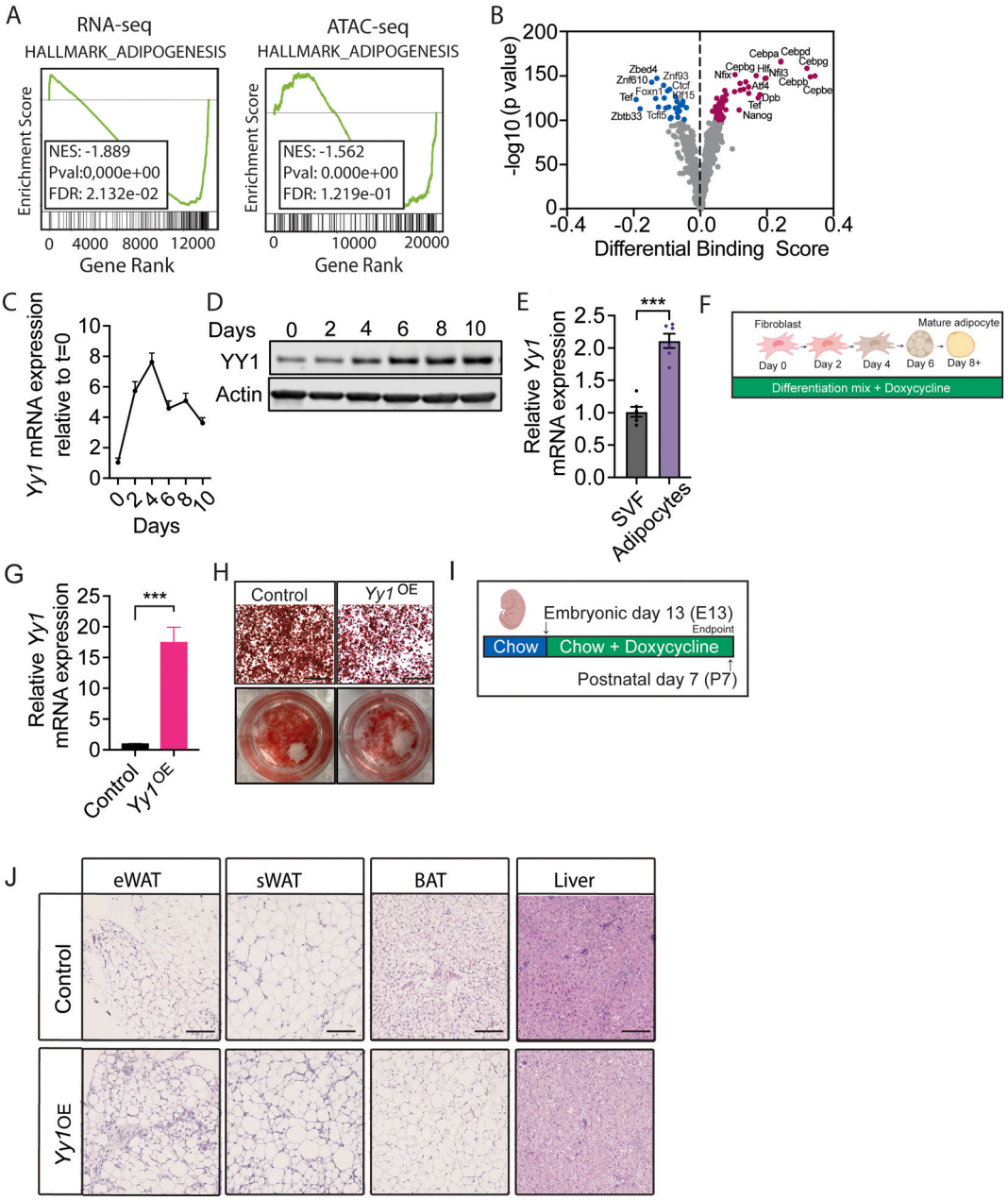

Fig. 6. Yy1 regulates preadipocyte hyperplasia *in vitro* and *in vivo*. **A)** Functional analysis of deregulated genes comparing eWAT transcriptomics from control *versus* $Yy1^{OE}$ ($n = 2$), and regions with differential chromatin accessibility in $Yy1^{OE}$ *versus* control adipocytes ($n = 3$) showed an enrichment of genes related to adipogenesis. **B)** Transcription factor occupancy as predicted by TOBIAS from control and $Yy1^{OE}$ ATAC-seq signals ($n = 3$ per group). **C—D)** Relative *Yy1* mRNA ($n = 3$) and YY1 protein expression at indicated timepoints during differentiation of wildtype SVF cells. **E)** Relative *Yy1* mRNA expression in RNA extracted from floated adipocytes *versus* SVF cells harvested from wild-type C57Bl6 mice ($n = 5$). **F)** Experimental outline of experiment designed to study the effect of *Yy1* induction on adipogenesis. SVF cells were collected from control and transgenic mice and differentiated *in vitro*, $n = 3$ per group. Doxycycline was added to cells at the time of differentiation stimulation (Day 0). **G)** Relative *Yy1* mRNA expression at Day 10 of differentiation/Doxycycline exposure. **H)** Lipid accumulation as detected by oil-red-o staining at Day 10 of differentiation/*Yy1* expression. Scalebar 100 μm. **I)** Experimental outline designed to study the effect of ectopic *Yy1* expression on hyperplasia *in vivo*. Doxycycline was administered at embryonic day 13, and tissues of interest collected at postnatal day 7. **J)** Representative images of histology evaluated by H&E of eWAT, SWAT, BAT and liver tissue collected from control or $Yy1^{OE}$ mice at postnatal day 7. (For interpretation of the references to colour in this figure legend, the reader is referred to the web version of this article.)

observed alterations in gene programs and phenotypes, we performed pathway analysis of differential peaks that mapped to promoter regions (Fig. 7D). Interestingly, fatty-acid metabolism or adipogenesis transcriptional networks were not amongst the top enriched pathways. Instead, there was an enrichment of pathways related to chromatin remodeling, DNA metabolic and repair processes, as well as ribonucleoprotein complex biogenesis, all of which correspond to previously reported YY1-controlled processes [4,12]. On the other hand, consistent with the observed increase in cell death after acute *Yy1* induction *in vivo*, there was an enrichment of genes connected to apoptotic signaling (Fig. 7D). As YY1 can act both as a transcriptional activator and repressor depending on the cell type and cellular context, we next integrated differential peaks in promoter regions with our RNA-seq data from eWAT. From our list of 1020 peaks with differential accessibility, only 53 displayed a significant differential transcriptional response between control and $Yy1^{OE}$ cells (p.adj < 0.05; Fig. 7E). Further filtering of

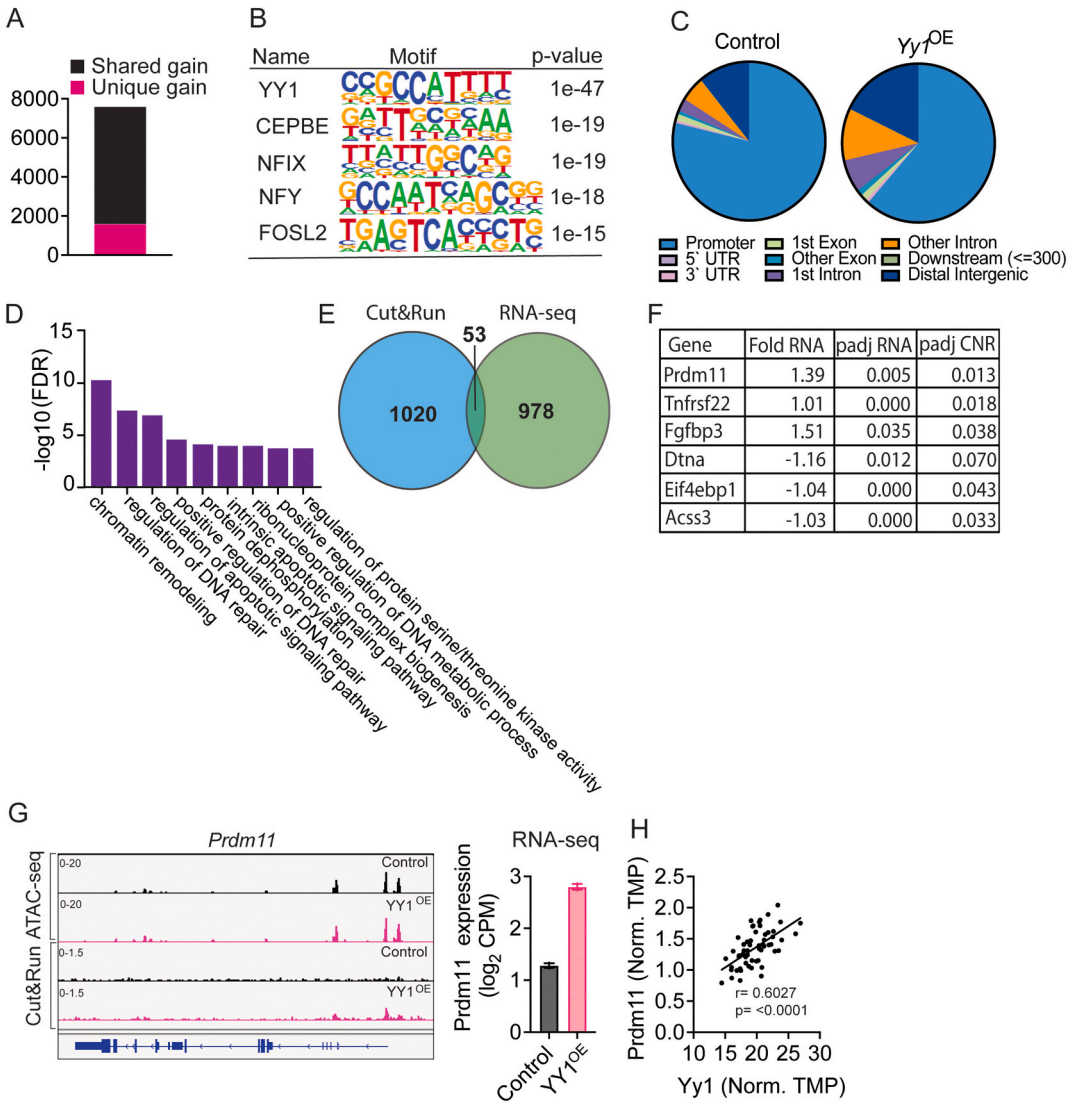

Fig. 7. Transcriptional responses induced by ectopic *Yy1* expression are partially mediated through direct binding to promoter regions. **A)** Number of shared (detected in both conditions, black) and unique (detected only in $Yy1^{OE}$, pink) YY1 binding sites. **B)** Top 5 *de novo* motifs called by HOMER for $Yy1^{OE}$ samples. **C)** Pie chart showing genomic annotation of called peaks of YY1 binding sites in control ($n = 3$) and $Yy1^{OE}$ ($n = 3$) samples. **D)** Pathway analysis of genes with increased YY1 binding in $Yy1^{OE}$ *vs.* control samples. **E)** Venn-diagram displaying number of promoter regions with differential YY1 binding signal (as identified by DiffBind from Cut&Run data) and differentially expressed transcripts (as determined by DESeq2 from RNAseq data) between control and $Yy1^{OE}$ conditions. **F)** Table showing genes with differential YY1 binding in promoter regions and expression level (log2Fc > 1 or < -1, p.adj < 0.05) in control *versus* $Yy1^{OE}$ samples. **G)** Representative Intergrated Genomic Viewer (IGV) tracks of normalized YY1 ATAC-seq and Cut&Run profiles around the Prdm11 locus in biological replicates of Control and $Yy1^{OE}$ samples. **H)** Pearson correlation analysis of YY1 and PRDM11 expression in human subcutaneous fat ($n = 57$). Data extracted from [32]. (For interpretation of the references to colour in this figure legend, the reader is referred to the web version of this article.)

YY1-bound promoters revealed three genes positively regulated by YY1 (log2Fc > 1, p.adj < 0.05) and three genes negatively regulated by YY1 (log2Fc < -1, p.adj < 0.057 (Fig. 7F). Although existing literature describing the function of these genes in adipocytes specifically is limited, data from other cell types have linked these potential YY1 targets to lipid and glucose metabolism (Fgfbp3 and Acss3) [21,22] and apoptosis (Tnfrsf22 and Prdm11) [23,24]. Of particular interest is the finding that induction of *Yy1* expression across the board caused increased binding to the promoter region, chromatin accessibility as well as transcription of Prdm11, a positive regulator of apoptosis (Fig. 7G). A positive correlation between Yy1 and Prdm11 transcriptional levels was confirmed in human subcutaneous fat (Fig. 7H). Collectively, our data suggest that the majority of observed transcriptional alterations induced by ectopic *Yy1* expression are not the result of classical activator/repressor functions acting on promoter regions directly, but are rather likely induced by other, thus far unexplored mechanisms in the adipocyte.

3. Discussion

By regulating food intake, energy expenditure, body temperature, insulin sensitivity and immune responses, adipose tissue plays a key role in whole-body physiology [13]. Maintaining vital adipocyte functions, such as metabolic plasticity (the balance between lipogenesis and lipolysis) and structural flexibility (hyperplasia/hypertrophy) is therefore crucial to sustain homeostasis. Here, we define the functional role of YY1 in several processes related to adipose tissue biology and expansion. We find that ectopic expression of YY1 controls adipose mass by negatively regulating adipocyte size (lipogenesis) and adipogenesis. Moreover, in an obese environment, acute YY1 expression in mature

adipocytes induces cell death and the accumulation of macrophages. Interestingly, as a transcription factor with many modes of action, we determine that the phenotypic alterations observed are not the result of differential binding to promoter regions of classical regulators of these processes. Instead, our data suggest that we should aim to better understand how gene regulation at distal sites and at the level of chromatin structure controls processes vital for adipose tissue homeostasis.

3.1. *Yy1 expression is tissue and context specific*

YY1 is expressed at high levels in adipocytes in both mice and humans. In human adipocytes, *YY1* expression is decreased in SWAT and VAT in response to obesity [17]. In mice, Yy1 expression is reduced in both stromal visceral cells and floated adipocytes isolated from HFD *versus* chow-fed mice. Analysis of human adipocytes suggests that *YY1* levels correlate with expression of canonical markers of mature adipocytes [17]. Regulation of *Yy1* expression appears to be tissue-specific; for example, *Yy1* is markedly upregulated in the liver of HFD-induced obese mice, where it plays a critical role in obesity-associated hepatosteatosis by repressing FXR expression [25]. These and our findings emphasize that YY1 transcriptional targets are highly cell-type specific.

3.2. *YY1 overexpression in adipose tissue triggers an unhealthy lean state*

In mice, the adipocyte-specific depletion or overexpression of YY1 cause a reduction of fat mass [15,16]. However, in contrast to $YY1^{OE}$ mice, YY1 knock-out mice display metabolic improvements. While YY1 overexpression leads to reduced fat mass, it is accompanied by insulin resistance, suggesting impaired adipose tissue expandability. Healthy adipose tissue expansion, particularly in the subcutaneous depot, is closely linked to insulin sensitivity and the capacity to safely store excess lipids [13]. In contrast, dysfunctional or fibrotic adipose tissue, which fails to expand adequately, redirects lipids to non-adipose tissues, promoting ectopic lipid accumulation and systemic insulin resistance. Thus, the YY1-overexpressing phenotype may reflect a metabolically unhealthy lean state, in which limited adipose storage capacity exacerbates metabolic dysfunction and liver steatosis despite reduced fat mass. This is further supported by our findings and previous studies showing that YY1 represses adipogenesis. The effects of loss of YY1 thus reduces adipose tissue mass by mechanisms distinct from the consequences induced by ectopic YY1 expression.

3.3. *Limited contribution of BAT to the Yy1 overexpression phenotype*

Verdeguer and colleagues report that YY1 induces alterations in the BAT secretome that could induce the shrinking of WAT by increasing energy expenditure [15]. With this observation in mind, we were curious to understand the relative contribution of BAT on our systemic phenotype. However, when overexpressing *Yy1* from the *Ucp1* promoter, we could not detect weight loss, reduction in white adipose tissue mass, nor metabolic defects. Our data thus suggest that gain of YY1 function regulates cellular processes that translate into a phenotype that is distinct from YY1 loss of function in BAT. When overexpressing *Yy1* (using both the adiponectin and *Ucp1* promoter), we did, however, observe a significant whitening of BAT, indicating local detrimental effects of high YY1 level in this tissue as well. Although beyond the scope of this paper, future experiments will need to clarify these effects and study the mechanisms of high YY1 levels in brown adipose tissue.

3.4. *YY1 mediates adipose tissue inflammation*

In line with our findings, Qiu *et al* describe an alteration in adipose tissue inflammation upon manipulation of YY1 expression [16]. They found that blocking YY1 reduced adipose inflammation, by reducing proinflammatory M1-like macrophages and the total number of macrophages in white adipose tissue depots. Furthermore, they discovered that YY1 null adipocytes secrete the anti-inflammatory polyamine spermidine to promote macrophage M2 polarization. Interestingly, blocking of spermidine production could reverse the resistance to HFD-induced metabolic dysfunctions in the knockout mice. Upon ectopic *Yy1* expression we find a significant increase in the total number of macrophages as well as the M1-like subtype. Although the accumulation of macrophages in this setting might be the result of the observed adipocyte death, the findings from Qiu and colleagues motivate us to examine whether YY1 induction promotes the secretion of signals from adipocytes that promote macrophage accumulation and M1 polarization.

3.5. *YY1 induces alterations in lipid metabolism gene expression*

Upon acute *Yy1* expression, we show that mature adipocytes repress transcriptional networks required for fatty acid biosynthetic pathways. Moreover, we noticed an overall loss of chromatin accessibility in promoter regions for genes involved in lipogenesis. In sum, this data suggests that the reduced transcriptional response might be the result of a loss of signaling rather than reflecting the accumulation of classical promoter-repressive signaling. Comparison of YY1 DNA-binding patterns between the two experimental conditions, as assessed by Cut&Run analysis, supports such a model. It is, therefore, likely that the observed effects are independent of direct YY1-promoter-binding, but instead, might the result of differential binding to, or regulation of other transcription factors and their co-activators/repressors involved lipid metabolism, as observed in other cell types [26,27]. Further experiments should focus on carefully characterizing the YY1-induced transcriptional alterations of lipid metabolism as well as adipogenesis related transcripts. In addition to performing assays to identify interaction partners (*e.g.* by ChIP-MS), it would be interesting to assess 3D chromatin conformation. Especially since peak annotation of differential binding analysis performed on the ATAC-seq data showed that most gain and loss peaks upon *Yy1* overexpression were found in distal intergenic regions and introns, not promoter regions. Also, of interest in relation to the regulation of 3D chromatin conformation, we found that ectopic expression of *Yy1* leads to reduced activity of the DNA looping factor CTCF (Fig. 5C). Interestingly, interactions between YY1 and CTCF were recently described in adipose tissue and suggested to regulate body fat distribution (apple *versus* pear shape) in women [28].

3.6. *YY1 regulates adipogenesis*

YY1 is an established regulator of developmental and differentiation processes in several cell types [4,6,7]. The data presented herein, as well as previously published computational and experimental data, suggest that YY1 also controls adipogenesis. A recent systematic analysis of gene expression data across four independent datasets identified YY1 to be amongst the top 10 critical transcription factors during adipogenic differentiation of mesenchymal stem cells [29]. Furthermore, the effect of manipulation of YY1 expression levels has previously been studied in a series of *in vitro* studies using the 3T3-L1 model system. Han and colleagues showed that YY1 overexpression decreased adipocyte differentiation, whereas Yy1 knockdown by RNA interference increased adipogenesis. The authors found YY1 to physically interact with two key transcription factors involved in adipogenesis, namely PPARγ and C/EPBP. In line with our data, they thus classified YY1 as a repressor of adipogenesis, and suggested the suppressive effects were mediated through repressing the activity of adipogenic transcription factors [30]. In contrast, Huang et al. suggested YY1 to be an adipocyte differentiation stimulator through suppressing CHOP-10, a dominant-negative family member of the C/EBP family of transcription factors [31].

4. Conclusion

Although the exact role of YY1 in the context of adipogenesis remains unclear, taking the current and previous reported *in vitro* data as well as

our *in vivo* data into consideration, it is obvious that YY1 levels need to be tightly controlled during the differentiation process. Future studies also taking 3D-related aspects of gene control into consideration, are needed to expand our insights into the mechanisms underlying adipocyte differentiation. Collectively, we describe the role of YY1 in regulating central aspects of adipocyte biology and add experimental evidence to what appears to be an understudied regulator of adipogenesis.

5. Materials and methods

5.1. Study design

The aim of this study was to assess the effect of adipocyte-specific Yy1 expression on systemic glucose metabolism. In controlled laboratory experiments, more than four mice were used in each treatment group based on standard deviations determined from previous studies. Mice were randomized after genotyping for the different treatments. Metabolic experiments had a predetermined end point based on length of high-fat diet feeding. For each experiment, mouse numbers, statistical tests, and experimental replicates are described in the figure legends. *In vitro* experiments were repeated at least three times, and the studies were not blinded. No data outliers were excluded. All protocols for mouse use and euthanasia were reviewed and approved by the Institutional Animal Care and Use Committee of the University of Texas Southwestern Medical Center (Animal Protocol # 2015-101207G).

5.2. Mice

Doxycycline-inducible, adipocyte-specific *Yy1*^{OE} mice were generated by crossing *TRE-Yy1* mice with adiponectin-rtTA or ucp1-rtTA mice. Mice were backcrossed with wild-type C57BL/6 J mice and genotyped by PCR (primers are listed in **Table S1**). In all experiments, mice were homozygous for adiponectin-rtTA or ucp1-rtTA and ± *TRE-Yy1*.

Mice were housed on a 12-h dark/light cycle at 22 °C, with *ad libitum* access to food (LabDiet #5058) and water. Mice were monitored daily, and cages changed every other week. Experiments were initiated at eight to ten weeks of age using littermates. The feeding regiment, number of animals, and duration of experiments is indicated in the Fig. s/Fig. legends. For special feeding, the following diets were used as indicated: chow diet + Doxycycline (600 mg/kg, Bio-Serv #S7123), HFD (60 % calories from fat, Bio-Serv #S1850), and HFD + Doxycycline (600 mg/kg Doxycycline, 60 % calorie from fat, Bio-Serv #S5867). All mice were fed doxycycline-containing diet to eliminate potential antibiotic-induced effects (including control animals).

5.3. Metabolic chamber studies

Metabolic chamber studies were performed by the UTSW metabolic Core Facility. Mice were single housed and acclimated in metabolic chambers for 5 days before the start of the experiment. The experiment was performed at room temperature (22 °C) on a 12-h dark-light cycle (7 am to 7 pm), and mice fed doxycycline-containing HFD and water *ab libitum*. A TSE calorimetric system was used to record food intake, locomotor activity, oxygen consumption and CO_2 production. Data was analyzed using CalR [33].

5.4. Body composition analysis

Total fat and lean mass were determined using the EcoMRI-100 whole body composition analyzer from Echo Medical Systems.

5.5. Systemic tests

Mice were fasted for 4 h prior to glucose and insulin tolerance tests. For oral glucose tests, dextrose (Sigma, D9434) was administered by oral gavage (2 mg/g body weight). Insulin (Humulin R) was given at 0.75 IU/kg by intraperitoneal injections. Glucose concentrations were determined at indicated timepoints using Bayer Contour glucometers. For the beta-3 adrenergic receptor agonist test, mice were not fasted. 1 mg/mL CL 316,243 (Sigma-Aldrich) was administered by intraperitoneal injection. Blood from the tail-vein was drawn at indicated timepoints, and serum obtained by centrifugation before it was kept frozen until further analysis.

5.6. Measurement of metabolites

Glycerol and NEFA were measured by free glycerol reagent (F6428, Sigma) and free fatty acid quantification kits (Wako Diagnostics-NEFA-HR2), respectively.

5.7. Hormone measurements

In accordance with the manufacturer's instructions, hormones were measured in serum samples from transgenic and control mice using the following kits: Mouse FGF21 (EZRMFGF21-26 K, Millipore), adiponectin (EZMADP-60 K, Invitrogen), leptin (#90080, Crystal Chem), and insulin (80-INSMS-E10, APLCO).

5.8. In vivo assessment of hyperplasia

Adipogenesis was examined in mice during the adipose tissue developmental stage as previously described [34]. After mating, mice were switched from normal chow to doxycycline (dox) chow on embryonic day 13 (E13). Adipose tissues were then collected at postnatal day 7 for histological analysis.

5.9. Histology

Tissues were fixed in formalin for up to 1 week at room temperature before stored in 50 % ethanol. Tissues were embedded in paraffin and 5 μm tick sections were used for H&E and immunofluorescent staining.

5.10. Tissue immunofluorescence (IF)

For tissue immunofluorescence, 5 μM tissue sections were deparaffinized and rehydrated before antigen retrieval was performed by boiling the sections in a pressure cocker at 98 °C for 12 min. For staining of iNOS, antigen retrieval was performed using Tris-based antigen unmasking solution, pH 9.0 (Vector Laboratories, H-3301) whereas antigen unmasking for F4/80 and cleaved caspase-3 was performed in sodium citrate buffer, pH 6.0 (Vector Laboratories, H-3300). After cooling to room temperature, sections for F4/80 and cleaved caspase-3 were blocked in 10 % normal goat serum (Invitrogen, 50197Z) and in 5 % Bovine serum albumin (BSA) diluted in PBS for sections stained with iNOS. Next, slides were stained overnight at 4 °C with primary antibodies; F4/80 (Cell Signaling, 70076) and cleaved-Caspase 3 (Cell Signaling, 9661) diluted 1:200 and iNOS (Abcam, ab15323) diluted 1:100. After washing (in PBS + 0.05 % Tween-20), samples were incubated with secondary antibodies (Alexa-Fluor 647: Invitrogen, A21244, Alexa-Fluor 546: Invitrogen, A11056) diluted 1:200 for one hour at room temperature in the dark. After washing three times for five minutes with PBS-0.05 % tween, samples were mounted with Prolong Diamond antifade reagent containing DAPI (Invitrogen, P36970). Images were obtained using an Olympus VS120 slide scanning system (40× objective). Images were quantified in QuPath. For iNOS and cleaved caspase-3, fluorescence signal was measured in 5 squares per mouse (area of each region of interest was 50,196 μM^2). For cleaved caspase-3, fluorescence signal was normalized to signal measured in a negative control slide (stained with secondary ab only). For F4/80, the number of macrophages were manually counted in 3 fields (each 660,734 μM^2) per mouse.

5.11. RNA isolation, cDNA synthesis, and quantitative RT-PCR

Tissues were homogenized in Trizol Reagent (ThermoFisher, Catalog number: 15596026) using a Qiagen Tissue lyser. After addition of chloroform, the resulting upper RNA containing aqueous phase was used as input for RNA extraction using the RNeasy Mini Kit from Qiagen (Product# 74104). RNA extraction from cells were performed according to the Qiagen protocol. Complementary DNA (cDNA) was next synthesized using the iScript cDNA synthesis kit from Bio-Rad. qRT-PCR was performed using primers (S1) and PowerUp SYBR Green Master Mix from Thermo Fisher Scientific (A25741) on the QuantStudio 6 Flex system (Thermo Fisher Scientific). The relative amount of cDNA was calculated by the $\Delta\Delta C_t$ method using mouse actin (m*Actin*) for normalization.

5.12. Western blotting

Cells were washed twice in ice-cold PBS, before scraped and lysed on ice for 20 min in Cell Lysis Buffer (Cell Signaling #9803) containing phosphatase and protease inhibitors (Thermo Fisher Scientific #78442). After centrifugation, protein concentrations were determined by BCA assay (Pierce BCA protein assay kit, Thermo Fisher Scientific) in the cleared supernatants. Proteins samples were immunoblotted using SDS-PAGE and transfer systems from Bio-rad using standard methods. YY1 expression was detected by incubating membranes overnight at 4 °C with anti-YY1 antibody (D5D9Z, Cell Signaling, #46395). Anti- β-actin (Sigma Aldrich) served as a loading control. Primary antibodies were detected by incubating with infrared-labeled secondary antibodies (Li-Cor) at room temperature for one hour. Blots were scanned on a Li-Cor Odyssey instrument.

5.13. Isolation of adipocytes and primary adipose stromal vascular cells

Inguinal fat pads were collected from 4 to 8 weeks old control and *Yy1*^{OE} mice. Four pads (two mice) were pooled per sample and cut into small pieces using scissors before digested in digestion buffer (1 mg/mL collagenase D supplemented with 1.5 % Bovine Serum Albumin (BSA) in Hanks Balanced Salt Solution (HBSS)). After 1–2 h digestion in a shaking water bath at 37 °C, cells were run through a 100 μm filter and washed twice with Fetal Bovine Serum (FBS)-containing media and centrifugation at 600 ×*g* for 5 min, 4 °C. Floating adipocytes were transferred to a new tube using a cut P1000 pipette tip. SVF cells were run through a second set of cell strainers (40 μm). Red blood cells were removed following the manufactures protocol (Sigma, R7757) before plating. Cells were cultured in DMEM/F12 + Glutamax (Gibo, 10565–018) supplemented with 10 % FBS, 2 mM Glutamax (Gibo, 35050) and 100 units/ug/mL Penicillin-Streptomycin (Gibo, 15140122).

5.14. Differentiation of stromal vascular cells and YY1 induction

Differentiation was induced 1 day after cells had reached confluency by adding the following differentiation cocktail: 5 μg/mL insulin (Sigma, I6634), 1 μM Dexamethasone (Sigma, D4902), 0.5 mM isobutylmethylxanthine (IBMX) (Sigma, I7018), and 1 μM Rosiglitazone (Sigma, R2408). Media was next renewed every other day by adding maintenance media containing 5 μg/mL insulin, starting 48 h after adding the induction cocktail. *Yy1* expression was induced by adding 0.5 μg/mL Doxycycline to the culture media.

5.15. Lipolysis assay in vitro

Lipolysis was measured in control and *Yy1*^{OE} adipocytes at differentiation day 9 (3 days post YY1 induction). Before addition of drugs, cells were primed in HBSS +1 % fatty-acid-free BSA for 2 h. Media was collected and snap-frozen for baseline measurements. Lipolysis was next stimulated by addition of 10 μM Forskolin (Sigma-Aldrich) or 5 μM CL 316,243 (Sigma-Aldrich). 4 h later media was collected and snap-frozen for subsequent glycerol measurements using the free glycerol reagent from Sigma (F6428).

5.16. RNAseq

RNA was isolated from eWAT as described above, and DNase-digestion performed on-column during the procedure using an RNase-free DNase set from Qiagen (79254) according to the manufacturer's protocol. RNA quality control, library generation and RNA-sequencing was performed by Novogene (Sacramento, CA, USA) on a Illumina Novaseq platform. DESeq2 was used to identify differentially expressed genes. Signed -log10 *p*-values were used as input for Gene set enrichment analysis (GSEA), and the analysis was performed in Python with GSEApy [34].

5.17. ATAC-seq

ATAC-seq was performed on *in vitro* differentiated adipocytes (differentiation day 9), 3 days post-YY1 induction (0.5 μg/mL doxycycline), using ATAC-Seq Kit from Active Motif (Cat# 53150). In brief, cells were carefully washed once in PBS before the addition of ATAC-lysis buffer. Cells were then lysed on ice for 10 min, before being collected and spun at 500 *g* at 4 °C for 10 min. Next, 100.000 cells were subjected for tagmentation according to the manufacturer's protocol. Tagmented DNA was amplified by PCR and libraries quality-checked using TapeStation. Libraries were sequenced on a NextSeq 2 K instrument. Preprocessing of ATAC-seq data was performed by the Genomics Core at UTSW. Differentially accessible regions were identified using DiffBind [35] with default settings, and annotated genome-wide to the closest transcription start site with ChIPseeker [36]. Peaks that mapped to promoter regions were extracted, and GSEA was performed using GSEApy [37]. Transcription factor footprints were detected with Transcription factor Occupancy prediction By Investigation of ATAC-seq Signal (TOBIAS, [38]). Additionally, motif enrichment analysis was performed with HOMER software [39] on differentially accessible peaks.

5.18. Cut and run

Cut and Run was performed on *in vitro* differentiated adipocytes using the Cut&Run Assay Kit from Cell Signaling (#86652) according to the manufacturer's recommendations. In brief, stromal vascular cells were isolated from subcutaneous fat from control and TRE-Yy1 mice as described above (section 5.13). To activate Yy1 expression, 0.5 mg/mL Doxycycline was added to the culture media at day 6 of differentiation. Cut&Run was performed on differentiated fully differentiated adipocytes (differentiation day 10). Cells were washed once in PBS, before scraped in cold Farnham Lysis Buffer (5 mM PIPES pH 8.0/85 mM KCl/ 0.5 % NP-40 + fresh DTT (1 mM) and complete protease inhibitor cocktail (Roche). Lysates were then spun at 5000 rpm, 4 °C for 5 min and the pellet resuspended in 100 uL lysis buffer. Samples were then processed as described from step II (Binding of Concanavalin A Beads and Primary antibody) in the protocol. Tri-methyl-Histone H3 (Lys4) (C42D8) (Cell Signaling, #9751) was used as a positive control whereas Rabbit (DA1E) mAb IgG XP Isotype Control served as a negative control. For mapping of Yy1 binding sites, samples were incubated in 0.1 μg YY1 (D5D9Z) Rabbit mAb (#46395) at 4 °C overnight. DNA was purified from input and enriched chromatin samples using the DNA purification kit from Zymo Research (D5205) and eluted in 25 μL total volume. DNA next was amplified by PCR, and libraries quality-checked using TapeStation. Libraries were sequenced on a NextSeq 2 K instrument. Preprocessing of CUT&RUN data was performed by The Genomics Core at UTSW. Differentially bound YY1 regions were identified using DiffBind, as previously described. Peaks were annotated with ChIPSeeker, and gene symbols were used as input for Gene Ontology (GO) analysis with

ClusterProfiler [40]. deepTools [41] was used to generate 1× normalized bigwig files. For visualization in Integrative Genomics Viewer (IGV) software, the non-specific IgG signal was subtracted from the YY1 signal using *bigwigCompare.* Motif enrichment analysis of YY1-bound regions was performed using HOMER.

5.19. Yy1 expression in human adipose tissue

Data was extracted from [32] (GEO accession: GSE159924), using GEOR2. Pearson correlation analysis was performed in GraphPad Prism using TMP values for all 57 samples available in the dataset. Two-tailed t-tests were performed to determine significance. Processed single-cell data for human adipose tissue were downloaded from Broad Institute's Single Cell Portal (SCP1376) and analysed with Seurat [42]. Cells annotated as adipocytes in the associated metadata were imported using Seurat's *CreateSeuratObject* function and separated by fat depot. Within each depot, per-cell YY1 expression was extracted and classified into "YY1-high" (above 75th percentile) and "YY1-low" (below 25th percentile). Differential expression between YY1-high and YY1-low was cells performed using Seurat's *FindMarkers* function (Wilcoxon rank-sum test; min.pct = 0.1, $\log_2$FC > 0.25; adjusted *p*-value < 0.05). The 25 most significant genes were displayed in heatmaps, and expression of key metabolic markers were shown in violin plots.

5.20. Statistics

Statistical analysis was performed using GraphPad Prism. Data is presented as mean + − standard error of the mean (SEM) unless otherwise stated. For *in vivo* experiments, each biological replicate represents an individual mouse. For experiments involving *in vitro* differentiated cells, each biological replicate is a pool of cells from two mice. Student t-test was used to compare control *versus Yy1* overexpression groups. Significance in the Figures is displayed as: *$P < 0.05$, **$P < 0.1$, *** $P \leq 0.001$.

CRediT authorship contribution statement

Line Pedersen: Writing – review & editing, Writing – original draft, Project administration, Methodology, Investigation, Formal analysis, Data curation. **Christy M. Gliniak:** Writing – review & editing, Project administration, Methodology, Investigation, Formal analysis, Data curation. **Thomas Myhre Dale:** Writing – review & editing, Methodology, Investigation, Formal analysis. **Qingzhang Zhu:** Methodology, Investigation. **Chao Li:** Methodology, Investigation. **Jan-Bernd Funcke:** Methodology, Investigation. **Clair Crewe:** Methodology, Investigation. **Jiahui Luo:** Investigation. **Lauren Palluth:** Investigation. **Yi Zhu:** Methodology, Investigation. **Philipp E. Scherer:** Writing – review & editing, Writing – original draft, Supervision, Funding acquisition, Conceptualization.

Consent for publication

Informed consent for publication was obtained from all participants.

Funding

This study was supported by US NIH grants RC2-DK118620, R01-DK55758, R01-DK099110, R01-DK127274 and R01-DK131537 to P.E.S. L.P. is supported by the European Union Horizon 2020 – Marie Skłodowska-Curie Actions (101026295).US NIH grant K01- DK131252 to C. M.G. US NIH grants R01-DK114036 and R00-DK122019 to C.C. US NIH grants R01DK136532 and R01DK136619 to Y.Z.

Declaration of competing interest

The authors declare that they have no known competing financial interests or personal relationships that could have appeared to influence the work reported in this paper.

Acknowledgments

We thank the UTSW Animal Resource Center, Histology Core, Metabolic Phenotyping Core, the Live Cell Imaging Core, Transgenic Core, and Flow Cytometry Facility for their excellent assistance with experiments performed in this paper. We thank Charlotte E Lee and Sambavi Elangovan for their invaluable contributions and expertise in histological techniques and quantitative PCR.

Appendix A. Supplementary data

Supplementary data to this article can be found online at https://doi.org/10.1016/j.metabol.2025.156439.

Data availability

All of the data included in this article are available if needed.

References

[1] Lam JC, Aboreden NG, Midla SC, Wang S, Huang A, Keller CA, et al. YY1-controlled regulatory connectivity and transcription are influenced by the cell cycle. Nat Genet 2024;56(9):1938–52.
[2] Cunningham JT, Rodgers JT, Arlow DH, Vazquez F, Mootha VK, Puigserver P. mTOR controls mitochondrial oxidative function through a YY1-PGC-1alpha transcriptional complex. Nature 2007;450(7170):736–40.
[3] Blattler SM, Verdeguer F, Liesa M, Cunningham JT, Vogel RO, Chim H, et al. Defective mitochondrial morphology and bioenergetic function in mice lacking the transcription factor yin Yang 1 in skeletal muscle. Mol Cell Biol 2012;32(16):3333–46.
[4] Zurkirchen L, Varum S, Giger S, Klug A, Hausel J, Bossart R, et al. Yin Yang 1 sustains biosynthetic demands during brain development in a stage-specific manner. Nat Commun 2019;10(1):2192.
[5] Varum S, Baggiolini A, Zurkirchen L, Atak ZK, Cantu C, Marzorati E, et al. Yin Yang 1 orchestrates a metabolic program required for both neural crest development and melanoma formation. Cell Stem Cell 2019;24(4):637–53. e9.
[6] Gabriele M, Vulto-van Silfhout AT, Germain PL, Vitriolo A, Kumar R, Douglas E, et al. YY1 Haploinsufficiency causes an intellectual disability syndrome featuring transcriptional and chromatin dysfunction. Am J Hum Genet 2017;100(6):907–25.
[7] Donohoe ME, Zhang X, McGinnis L, Biggers J, Li E, Shi Y. Targeted disruption of mouse yin Yang 1 transcription factor results in peri-implantation lethality. Mol Cell Biol 1999;19(10):7237–44.
[8] Thomas MJ, Seto E. Unlocking the mechanisms of transcription factor YY1: are chromatin modifying enzymes the key? Gene 1999;236(2):197–208.
[9] Sarvagalla S, Kolapalli SP, Vallabhapurapu S. The two sides of YY1 in Cancer: a friend and a foe. Front Oncol 2019;9:1230.
[10] Faulk CD, Kim J. YY1's DNA-binding motifs in mammalian olfactory receptor genes. BMC Genomics 2009;10:576.
[11] Rao A, Hero 3rd AO, States DJ, Engel JD. Motif discovery in tissue-specific regulatory sequences using directed information. EURASIP J Bioinform Syst Biol 2007;2007(1):13853.
[12] Verheul TCJ, van Hijfte L, Perenthaler E, Barakat TS. The why of YY1: mechanisms of transcriptional regulation by yin Yang 1. Front Cell Dev Biol 2020;8:592164.
[13] Sakers A, De Siqueira MK, Seale P, Villanueva CJ. Adipose-tissue plasticity in health and disease. Cell 2022;185(3):419–46.
[14] Luo L, Liu M. Adipose tissue in control of metabolism. J Endocrinol 2016;231(3):R77–99.
[15] Verdeguer F, Soustek MS, Hatting M, Blattler SM, McDonald D, Barrow JJ, et al. Brown adipose YY1 deficiency activates expression of secreted proteins linked to energy expenditure and prevents diet-induced obesity. Mol Cell Biol 2015;36(1):184–96.
[16] Qiu C, Lu Y, Wu S, Guo W, Ni J, Song J, et al. Blocking adipocyte YY1 decouples thermogenesis from beneficial metabolism by promoting spermidine production. Diabetes 2025;74(3):295–307.
[17] Emont MP, Jacobs C, Essene AL, Pant D, Tenen D, Colleluori G, et al. A single-cell atlas of human and mouse white adipose tissue. Nature 2022;603(7903):926–33.
[18] Han MS, White A, Perry RJ, Camporez JP, Hidalgo J, Shulman GI, et al. Regulation of adipose tissue inflammation by interleukin 6. Proc Natl Acad Sci USA 2020;117(6):2751–60.
[19] Lu G, Zhang R, Geng S, Peng L, Jayaraman P, Chen C, et al. Myeloid cell-derived inducible nitric oxide synthase suppresses M1 macrophage polarization. Nat Commun 2015;6:6676.
[20] Wang QA, Tao C, Gupta RK, Scherer PE. Tracking adipogenesis during white adipose tissue development, expansion and regeneration. Nat Med 2013;19(10):1338–44.

[21] Tassi E, Garman KA, Schmidt MO, Ma X, Kabbara KW, Uren A, et al. Fibroblast growth factor binding protein 3 (FGFBP3) impacts carbohydrate and lipid metabolism. Sci Rep 2018;8(1):15973.
[22] Wang L, Yuan H, Li W, Yan P, Zhao M, Li Z, et al. ACSS3 regulates the metabolic homeostasis of epithelial cells and alleviates pulmonary fibrosis. Biochim Biophys Acta Mol basis Dis 2024;1870(2):166960.
[23] Schneider P, Olson D, Tardivel A, Browning B, Lugovskoy A, Gong D, et al. Identification of a new murine tumor necrosis factor receptor locus that contains two novel murine receptors for tumor necrosis factor-related apoptosis-inducing ligand (TRAIL). J Biol Chem 2003;278(7):5444–54.
[24] Fog CK, Asmar F, Come C, Jensen KT, Johansen JV, Kheir TB, et al. Loss of PRDM11 promotes MYC-driven lymphomagenesis. Blood 2015;125(8):1272–81.
[25] Lu Y, Ma Z, Zhang Z, Xiong X, Wang X, Zhang H, et al. Yin Yang 1 promotes hepatic steatosis through repression of farnesoid X receptor in obese mice. Gut 2014;63(1):170–8.
[26] Li Y, Kasim V, Yan X, Li L, Meliala ITS, Huang C, et al. Yin Yang 1 facilitates hepatocellular carcinoma cell lipid metabolism and tumor progression by inhibiting PGC-1beta-induced fatty acid oxidation. Theranostics 2019;9(25):7599–615.
[27] Pan G, Diamanti K, Cavalli M, Lara Gutierrez A, Komorowski J, Wadelius C. Multifaceted regulation of hepatic lipid metabolism by YY1. Life Sci Alliance 2021;4(7).
[28] Erdos E, Sandor K, Young-Erdos CL, Halasz L, Smith SR, Osborne TF, et al. Transcriptional control of subcutaneous adipose tissue by the transcription factor CTCF modulates heterogeneity in fat distribution in women. Cells 2023;13(1).
[29] Dai M, Hong W, Ouyang Y. Identification and validation of hub genes and construction of miRNA-gene and Transcription factor-gene networks in Adipogenesis of mesenchymal stem cells. Stem Cells Int 2024;2024:5789593.
[30] Han Y, Choi YH, Lee SH, Jin YH, Cheong H, Lee KY. Yin Yang 1 is a multi-functional regulator of adipocyte differentiation in 3T3-L1 cells. Mol Cell Endocrinol 2015;413:217–27.
[31] Huang HY, Li X, Liu M, Song TJ, He Q, Ma CG, et al. Transcription factor YY1 promotes adipogenesis via inhibiting CHOP-10 expression. Biochem Biophys Res Commun 2008;375(4):496–500.
[32] Beals JW, Smith GI, Shankaran M, Fuchs A, Schweitzer GG, Yoshino J, et al. Increased adipose tissue Fibrogenesis, not impaired expandability, is associated with nonalcoholic fatty liver disease. Hepatology 2021;74(3):1287–99.
[33] Mina AI, RA LeClair, KB LeClair, Cohen DE, Lantier L, Banks AS. Calr: a web-based analysis tool for indirect calorimetry experiments. Cell Metab 2018;28(4):656–66.e1.
[34] Zhu Q, Chen S, Funcke JB, Straub LG, Lin Q, Zhao S, et al. PAQR4 regulates adipocyte function and systemic metabolic health by mediating ceramide levels. Nat Metab 2024;6(7):1347–66.
[35] Stark R, B G. DiffBind: Differential Binding Analysis of ChIP-Seq Peak Data. http://bioconductororg/packages/release/bioc/vignettes/DiffBind/inst/doc/DiffBindpdf; 2011.
[36] Wang Q, Li M, Wu T, Zhan L, Li L, Chen M, et al. Exploring epigenomic datasets by ChIPseeker. Curr Protoc 2022;2(10):e585.
[37] Fang Z, Liu X, Peltz G. GSEApy: a comprehensive package for performing gene set enrichment analysis in Python. Bioinformatics 2023;39(1).
[38] Bentsen M, Goymann P, Schultheis H, Klee K, Petrova A, Wiegandt R, et al. ATAC-seq footprinting unravels kinetics of transcription factor binding during zygotic genome activation. Nat Commun 2020;11(1):4267.
[39] Heinz S, Benner C, Spann N, Bertolino E, Lin YC, Laslo P, et al. Simple combinations of lineage-determining transcription factors prime cis-regulatory elements required for macrophage and B cell identities. Mol Cell 2010;38(4):576–89.
[40] Yu G, Wang LG, Han Y, He QY. clusterProfiler: an R package for comparing biological themes among gene clusters. OMICS 2012;16(5):284–7.
[41] Ramirez F, Dundar F, Diehl S, Gruning BA, Manke T. Deeptools: a flexible platform for exploring deep-sequencing data. Nucleic Acids Res 2014;42(Web Server issue):W187–91.
[42] Hao Y, Stuart T, Kowalski MH, Choudhary S, Hoffman P, Hartman A, et al. Dictionary learning for integrative, multimodal and scalable single-cell analysis. Nat Biotechnol 2024;42(2):293–304.